Reverse-Correlation Analysis of Mechanosensation Circuit in *C. elegans* Reveals Temporal and Spatial Encoding

Daniel A. Porto[1], John Giblin[2], Yiran Zhao[2], Hang Lu[1,2,*]

[1]Interdisciplinary Bioengineering Program, Georgia Institute of Technology, USA

[2]Department of Biomedical Engineering, Georgia Institute of Technology, USA

*Correspondence should be addressed to HL: hang.lu@gatech.edu, 1-404-894-8473

Abstract

Animals must integrate the activity of multiple mechanoreceptors to navigate complex environments. In *Caenorhabditis elegans*, the general roles of the mechanosensory neurons have been defined, but most studies involve limited types of stimuli, potentially biasing the characterization. Here, we formulate unbiased descriptions of the mechanosensory system by using reverse correlation analysis. We use a custom tracking, selective illumination, and optogenetics platform to compare two mechanosensory systems: the gentle-touch and harsh-touch neurons. This method yields linear filters that capture dynamics, consistent with previous findings, as well as new insights on the spatial encoding. Our results suggest that the tiled network of the gentle-touch neurons has better resolution for spatial encoding than the harsh-touch neurons. Additionally, linear-nonlinear models accurately predict behavioral responses based only on sensory neuron activity. Our results capture the overall dynamics of behavior induced by the activation of sensory neurons, providing simple transformations that fully characterize these systems.

Main Text

A key function of the nervous system is to integrate the activity from a variety of sensory neurons and transform these neuronal signals into specific behavioral responses. This integration occurs not only across sensory modalities but also within a single modality such as in mechanosensation; animals must integrate information from spatially distributed mechanoreceptor neurons throughout their body to determine where and how they have been stimulated [1]. *Caenorhabditis elegans*, a nematode with a mapped connectome and powerful genetic and physiology tools, is an effective model organism for investigating relationships between sensory inputs and downstream activity [2,3]. The components of the neural circuits involved in *C. elegans* mechanosensation have been elucidated through various genetic and behavioral analyses coupled with neuronal cell ablation assays [4,5]. Two sets of mechanoreceptors are specifically responsible for sensing touch throughout the body: the gentle touch sensing TRNs and harsh touch sensing PVDs [6]. These neurons are well studied, and quantitative aspects such as temporal dynamics , spatial precision, and behavior stochasticity have been characterized [7–11]. However, most descriptions are specific to a single specific input stimuli, typically a single pulse with an eye lash or a metal pick. This leads to descriptions that are biased toward explaining only this unnatural stimulus, and do not allow for the overall prediction of the systems to novel stimuli. To elucidate the complete transformations between mechanoreceptor neurons and behavioral outputs, we sought to describe these transformations in an unbiased quantitative framework that captures the systems' dynamics in high spatial and temporal resolution.

A successful technique for characterizing neuronal activity in several model systems is the use of reverse correlation analysis with a white noise stimulus [12–19]. Reverse correlation is commonly applied in sensory physiology to model a sensory neuron's response to natural stimuli as a linear filter. The computed linear filters provide a complete description of the linear dynamics of the neuron, and can be used in conjunction with a nonlinear filter to accurately model its function [14,20–23]. This technique has also been extended to modeling behavior in Drosophila larvae, where computed filters enabled accurate modeling of locomotion dynamics in response to activating chemosensory neurons [24–27]. In *C. elega*ns, reverse correlation has been applied to the chemosensory neurons ASH and AWC by applying a pseudorandom chemical stimulus, revealing temporal dynamics that control downstream chemotactic behavior [28]. This technique is also ideal for the characterization of mechanosensory circuit dynamics in *C. elegans*, particularly for quantifying and contrasting the spatial and temporal properties of the gentle and harsh touch neurons.

Although reverse correlation analysis allows for accurate estimations of system dynamics, several experimental obstacles hinder its applicability to the mechanosensory circuits in *C. elegans* at present. Current techniques for delivering precise mechanical stimuli to animals involve the delivery of a mechanical force via a stylus or microfluidic device to specific locations on the animal's body [29–32]. Although ideal for neuronal imaging, these techniques require the immobilization of animals with glue or other techniques, and therefore, do not allow for reverse correlation analysis with behavior response dynamics. Additionally, many of these techniques have a low experimental throughput, and cannot provide the large sample sizes required for reverse correlation studies. One technique that overcomes these challenges is the use of optogenetics, as a light stimulus is more easily controlled, and can be used to activate specific neurons in freely moving animals [26,27,33]. This fictive stimulus has the added benefit of bypassing differences in receptor protein expressions, allowing for comparison between sensory systems. In order to apply light stimuli with spatial resolution to activate specific regions of sensory neurons, we adapted a previously developed tracking platform with selective illumination [34]. The custom microscopy system uses a projector and computer vision tools to track the animal, allowing for the delivery of spatially and temporally resolved stimuli required for white noise signal delivery.

In this work, we developed an experimental approach for performing white noise analysis on *C. elegans*, and apply this method to elucidate the mathematical transformations between mechanosensory neuron activity and behavioral response. Using our platform, we computed linear filters that characterize the dynamics of the gentle touch sensing TRNs and harsh touch sensing PVDs. These filters provide a quantitative framework for the functions of these neurons, and allowed for the investigation of differences in spatial encoding. Furthermore, this method allowed us to create models that accurately predict behavioral changes in response to mechanosensory neuron activity. Our method provides simple transformations that fully characterize these systems by capturing the spatiotemporal dynamics of behaviors induced by optogenetic activation of sensory neurons.

Results

Reverse-correlation analysis using optogenetics and behavior tracking

We characterize and compare the dynamics for two distinct sets of mechanosensory neurons: the gentle touch sensing TRNs and the harsh touch sensing PVDs (Figure 1A). To fully capture the dynamics of *C.*

elegans' behavioral response downstream of mechanosensory neuron activity using reverse correlation, two experimental requirements are the delivery of a white noise input and accurate measurements of the output. To probe the circuit, we used optogenetics to directly activate the mechanosensory neurons with a white noise signal. This unmediated input enabled us to activate neurons regardless of expression of mechanotransductive channels. This allows the comparison of how the two systems and their morphologies control downstream activity, rather than differences in their sensory activation. Additionally, whereas a natural stimulus can activate additional sensory neurons and possibly interfere with the characterization, the optogenetic stimulus will only activate the neurons expressing channelrhodopsin. Therefore, the resulting filters characterize the dynamics of behaviors exclusively in response to specific neurons. Our tracking platform [34] enables the delivery of patterned illumination while simultaneously tracking individual animals, allowing for selective activation of specific sections of transgenic animals with high spatial and temporal precision (Figure 1B, Supplemental Movie 1, Methods). We used this platform to deliver the white noise light stimulus for reverse correlation; we activate mechanosensory neurons in a pseudorandon m-sequence pattern, a spectrally unbiased binary signal (Methods).

Provided the optogentic stimuli as input, the outputs we seek to characterize are the behavioral responses of animals. In order to analyze the animals' behavior in a high-throughput and unbiased manner, we developed a custom MATLAB script (Methods). The worm's posture and position are extracted for each frame, which are then used to quantify various "continuous" behaviors such as instantaneous velocity, instantaneous head angle, and instantaneous acceleration (Figure 1C). In addition to these "continuous" behaviors we also quantified and categorized several classical "discrete" behaviors such as reversals, pauses, and omega turns [35–38] (Figure 1C, Methods). Each of these continuous and discrete variables were used as separate outputs for reverse correlation analysis, yielding separate filters for any given stimulus pattern. By computing filters for a large portion of the worm's behavioral repertoire, we can describe the overall behavioral response when stimulating specific mechanosensory neurons.

To apply reverse correlation, we use a white noise light stimulus for optogenetics and quantified behavioral responses to model *C. elegans* response as transformations of linear and non-linear filters. When characterizing mammalian neuronal systems, a neuron's response is modeled by computing the average of the stimuli that preceded its action potentials (spike-triggered average or STA) or its subthreshold voltages (voltage-weighted average or VWA) [22]. Similarly, we estimate the dynamics of *C.*

elegans response by computing the behavior weighted average of the stimulus (BWA). When stimulating specific segments of the mechanosensory systems, the BWA represents how the animals characteristically transform patterns of activity of those neurons into specific behaviors, providing a filter estimation of this transformation (Figure 1D).

In order to accurately estimate these linear filters, a large sample size is required to test enough input values [13,23]. To identify the sample size required in our system, we characterized the speed of convergence of computed filters as the number of input samples increased. We compared subsequent filters by computing the L2 norm of their differences, and found that the filter converges (to a relative tolerance of $\delta<0.005$) after using roughly 30,000 frames of tracking data (Figure 1E, Supplemental Movie 2). With our experimental conditions, this is equivalent to a sample size of roughly 30 animals (Methods).

Linear Filters for anterior and posterior touch receptor neurons (TRNs) capture robust and repeatable dynamics

We first used our method to characterize responses to the touch receptor neurons (TRNs: ALML/R, AVM, PVM, and PLML/R) by using transgenic animals expressing channelrhodopsin (ChR2) under the *mec-4* promotor (Methods)[34]. In response to natural stimuli, the posterior TRNs (PVM and PLML/R) respond to posterior touch, inducing a forward acceleration, whereas the anterior TRNs (ALML/R and AVM) respond to anterior touch, inducing a reversals [4,6,10,34,39]. To characterize the dynamics of these responses, we applied an m-sequence light stimulus to either the anterior or posterior region of transgenic animals, selectively stimulating the anterior or posterior TRNs, respectively. We first computed linear filters characterizing the relationship between anterior TRNs and both discrete and continuous behaviors (Figure 2B, F, supplementary figure 1). We performed experiments with control animals that were not fed all trans-retinol (ATR), a cofactor required for ChR2 function. Compared to the control animals, the BWA for the acceleration of worms that were fed ATR results in a filter with a robust negative peak (-13 ± 0.50 $\mu m/s^2$), indicating that activating the anterior TRNs induces a negative change in acceleration. This direction in change of acceleration is expected from the negative acceleration present in reversal responses. In contrast, the computed filters for control animals are flat, zero-mean signals (Figure 2, gray lines), indicating that the computed filters for ATR animals are due only to the activation of the anterior TRNs, and not due to spontaneous behaviors. In addition to validating the direction of acceleration to activation of anterior TRNs, our method also reveals new information about the dynamics of these

responses: metrics such as the delay to the peak (0.2s) and the decay rate of the filter (0.4s) reveal the characteristic dynamics of an animal's acceleration in response to activity in the anterior TRNs. In comparison, the BWA computed with velocity also returns a linear filter with a negative peak (-6.1 ± 0.39 µm/s), although with a slower peak (0.7s) and longer decay (0.6s) (supplementary figure 1). This suggests that although animals reverse for a relatively long time after the stimulus (1.3s), the deceleration portion of this reversal only takes place in the first 0.6s after a stimulus.

In addition to continuous signals, we also estimated linear filters for the probability of transitions between defined states. Instead of predicting specific values, filters computed for these behaviors indicate a change in probability of transitions to specific behaviors. When computing the BWA with transitions into pauses or reversals in response to anterior TRNs, we observe a linear filter with a clear positive peak ($3.0 \times 10^{-3} \pm 2.6 \times 10^{-4}$), with a delay of 0.4s and decay of 0.3s (Figure 2F). This indicates that activating the TRNs induce an increase in probability of those transitions, and this increased likelihood happens within the first second after a stimulus.

Furthermore, to ensure that the computed linear filters are indeed characteristic of the system and not an artifact from the input signal itself, we delivered a different m-sequence signal to the same anterior region of the worm (Figure 2 C, G, supplementary figure 1). By computing the reverse correlation to various behavioral responses in these trials, we observe similar linear filters to those obtained from the previous trial, with no statistical difference between filter peak values (Figure 2 C, G, E, I, supplementary figure 1). These results demonstrate that the linear filters are indeed characteristic of *C. elegans*' behavioral output specifically in response to the activity in the anterior TRNs.

Next, we sought to compare the dynamics of the animals' response between anterior or posterior TRN activities. Previous findings have shown that applying a mechanical force to the posterior region of the animal induces an acceleration, and PLM is required for these responses [4,6,10]. As with the anterior TRNs, we stimulated the posterior TRNs by applying an m-sequence light stimulus to the posterior half of the animal, and computed the BWA for the same quantified behaviors (Figure 2 D, H, supplementary figure 1). The filter for acceleration has a positive peak (2.8 ± 0.48 µm/s^2), but have much smaller magnitudes than their anterior counterparts and are not statistically different from control animals (Figure 2D). Similarly, the filter computed for transitions into pauses and reversals has a negative peak ($-1.3 \times 10^{-3} \pm 2.5 \times 10^{-4}$), although not statistically different from control animals (Figure 2H, I). Interestingly, although

the computed linear filters for the posterior TRNs have peaks in the directions that are consistent with literature, they were close to zero-mean and suggest a low rate of these responses when activating PLM and PVM.

Reverse Correlation Analysis of Harsh Touch Sensing PVD Neurons

In addition to the TRNs, *C. elegans* has another set of neurons that are responsible for body touch sensation. The PVD neurons are morphologically unique sensory neurons that have extensive and organized dendritic structures that expand most of the body of the worm. Similar to the TRNs, they have processes that expand the body and are responsive mechanical stimuli, although they response to different types of stimuli (harsh touch) [5,7–9,11]. Additionally, although both systems have processes that expand the body, they apply different strategies to cover this large area (Figure 1A). The TRNs employ a tiled network, with neurons consisting of a singular axon are spread out along the body of the animal. In comparison, the PVDs employ a branched network, with two centralized cell bodies, and each neuron has an extensive dendritic branch that expands a side of the animal. To investigate whether these differences in morphology affected downstream activity, we applied the same reverse correlation method to animals expressing ChR2 in the PVD neurons [11].

For comparison with the TRNs, we similarly divided the stimulus regions into anterior and posterior segments, and computed the BWA and estimated linear filters for the same behaviors. Compared to the linear filters from TRN activation, the computed filters for PVD activation are entirely different (Figure 3, supplementary 2). When computing the BWA for acceleration or velocity, both the anterior and posterior segments produced filters with positive peaks near t=0, indicating that activating either the anterior or posterior segments of PVD dendrites induces an increase in velocity. However, the filters from the posterior segment are more robust, with a higher positive peak for both the acceleration (4.0 ± 0.58 µm/s^2 vs 7.1 ± 0.58 µm/s^2) and velocity (3.5 ± 0.32 µm/s vs 7.1 ± 0.32 µm/s) filters (Figure 3B, C, D, supplementary figure 2). This clear contrast from the TRN filters suggests a different role for PVD sensory neurons in the behavioral circuit – that PVD activation promotes acceleration, and TRNs promote reversals, consistent with previous findings [9,10].

Additionally, in contrast to those for the TRNs, the posterior PVD acceleration filters have a very strong refractory portion, indicated by the negative peaks following the positive peaks; the magnitudes of the

negative peaks are of similar values to the first positive peak (Figure 3D). This suggests that in comparison to the reversal responses when activating the anterior TRNS, the acceleration in response to PVD activation has a much longer adaptation period, preventing subsequent accelerations.

We also estimated the anterior and posterior PVD linear filters for the probability of transitions between defined states. Not surprisingly, when computing the BWA with transitions into pauses or reversals in response to either anterior or posterior PVD, we observe flat, zero-mean linear filters (Figure 3 E, F). The filters are statistically indifferent from control group (Figure 3G), indicating that activation of the PVDs do not induce a change in probability of these events.

Linear-Nonlinear Models Predict Behavioral Response

The linear filters computed from BWA in response to a white noise signal capture the linear dynamics of the analyzed systems. However, biological systems are rarely purely linear [17]. Indeed, modeling the mechanosensory systems purely as linear filters computed from BWA does not fully predict behavioral responses to sensory neuron activation (Supplementary Fig. 3a). A common approach for modeling the nonlinear dynamics of a system is to use a linear-nonlinear cascade, where a static nonlinear filter is used to characterize the nonlinear dynamics not captured by reverse correlation [13,16–18]. To define static nonlinear filters, we compared predicted outputs from each previously computed linear filter with measured experimental outputs (Methods). We first computed the static filters for behavioral responses to anterior TRNs. We compared the quantified behavioral responses to the predictions based on the linear filters and observed positive correlations between predicted and experimental outputs, indicating that the linear model does indeed capture much of the dynamics in these responses (Figure 4 A, B, gray circles). To mathematically characterize the static filters, we used quadratic functions to describe the relationship between linear prediction and experimental measurements (Figure 4 A, B blue lines, Methods). The quadratic functions accurately model these relationships, indicating that they capture a large portion of the nonlinear dynamics of the anterior TRNs. We also computed a static nonlinear filter for each linear filter computed for the posterior TRNs. In contrast to the anterior TRNs, there is no clear correlation between experimental measurements and predicted values (Figure 4C, D). This is expected, as the estimated linear filters for these neurons were close to zero-mean, yielding a small range of predicted responses. Furthermore, because the linear filters alone led to a low predictability of responses for

posterior TRNs, nonlinear functions also fail to capture a large portion of the variability (Fig 4 C, D, orange lines).

To test the accuracy of computed linear-nonlinear (LN) cascade models in predicting behavioral responses to novel stimuli, we probed the anterior TRNs with a different m-sequence stimulus (Figure 5A, Methods). We first compared the velocities of animals predicted from the LN models with the quantified velocities in each trial (Supplementary Fig. 1b). Although the magnitude of predicted velocity from the model did not exactly match the experimental measurements, the model accurately predicts average changes in velocity in response to this novel stimulus. Not surprisingly, we find that although the model accurately predicts the average behavioral response, it fails to accurately predict responses on a single-trial basis (Figure 5B). This suggests that behavioral responses to stimuli are intrinsically stochastic, but our model captures average responses that are stereotypical to activating the anterior TRNs. Further, in addition to predicting the continuous velocity of the animals, the LN model for reversals also predicts increases in probability of transitions into the distinct response (Supplementary Fig. 4).

Although the LN models generally predict behavioral dynamics, a key discrepancy between model predictions and experimental measurements is the lack of adaptation to the stimulus. In our experiments, we observe a time-dependent decrease in the magnitude of responses, which fails to be captured in either the dynamic linear filter or the static nonlinear filters. Biologically, this habituation of responses is commonly observed in sensory systems [40]. In order to model this decay of responses, we apply a dynamic exponential function following the LN cascade. We tested a wide range of decay rate values in the model, and found that a decay rate of 50s best captured the observed responses (Supplementary Fig. 5). Interestingly, this decay rate is consistent with findings from experiments investigating habituation to optogenetic stimulation of TRNs [41]. When adding this exponential component, the accuracy of our model's predictions of behavioral responses improve for later time points, improving the overall accuracy of our models (Figure 5 B,C). Our results illustrate how the linear filters computed from BWA, when combined with additional nonlinear filters, can accurately predict behavioral responses to sensory neuron activation.

Spatially Refined Selective Illumination Improves Resolution of Linear Filters from BWA

We have thus far characterized mechanosensory systems by probing either the anterior or posterior segments of the animal, similar to previous investigations of the receptive fields of mechanosensory

systems [9,31]. To further examine the spatial resolution of the mechanosensory systems, we took advantage of our light stimulus, which allows for the probing of specific spatial segments as small as 14µm [34]. We characterized the TRN system with better resolution by increasing the number of segments in our stimulus to 4 (Fig. 6, Supplementary Fig. 6). This segmentation of the body allows for the computation of separate linear filters for the cell bodies of posterior PVM and PLM (while keeping a high number of photons in the stimulus region). We applied an m-sequence stimulus selectively to one of the four segments, and computed linear filters for both continuous and discrete behavioral outputs. The filters computed for acceleration in response to stimulating four segments were similar to two segments. When activating the most anterior quarter and second most anterior quarter, the linear filters have a prominent negative peak, similar to the filter computed from stimulating the entire anterior region (compare Figure 6 B, C, F and Figure 2 B,C,E). Similarly, when computing the BWA with acceleration in response to the most posterior quarter, which includes the PLM cell bodies, and second most posterior quarter, which contains the PVM cell body, the resulting linear filters are flat, with no significant difference from control animals (Figure 6 D, E, F). These filters are also similar to the flat filter computed from stimulating the entire posterior region (Figure 2 D, E).

In contrast to the acceleration filters, when computing linear filters with transitions into pauses or reversals, we find differences in spatial encoding. The results for the anterior segments were similar to acceleration, with the resulting filters for the most anterior quarter and second-most anterior quarter having positive peaks similar to the filter computed when stimulating the entire anterior regions (compare Figure 6 G, H, K to Fig2 F, H, I). This suggests that there is low spatial encoding of activity in the anterior TRNs. In contrast with the anterior region, dividing the posterior segment of the TRNs separates the cell bodies of PVM and PLM is different filters. The filter for the most posterior quarter was again very similar to the flat filter computed when stimulating the entire posterior region (Figure 6J). Interestingly, the filter for second-most posterior quarter has a negative peak close to t=0 (Fig 6 I, K), indicating that there is a reduced probability of pauses and reversals when activating PVM. This suggests that PVM has a previously undescribed function of inhibiting pauses and reversals. Additionally, this implies that there is spatial encoding of activity in the posterior TRNs: filters computed when activating either of the PVM or PLM cell bodies encode for different responses.

Discussion

The nervous system continuously transduces sensory stimuli into layers of neural activity and appropriate behavioral outputs. One of the biggest challenges in mapping this neuronal encoding is the lack of experimental and computational methods that provide a quantitative framework for characterizing how a layer of neural activity is transduced into the downstream circuit. In this work, we use reverse correlation analysis with a custom tracking platform to investigate the spatial and temporal encoding of two mechanosensory systems, the gentle touch sensing TRNs and the harsh touch sensing PVDs. We computed several linear filters that quantitatively describe transformations between sensory neuron activity and behavioral outputs, and support previous findings about the systems. Analysis of the PVDs produced linear filters that indicate an increase in velocity and acceleration from their activation, which is consistent with literature on its function [5,7–9,11]. Similarly, the linear filters computed for the TRNs were also consistent with previous literature, as the anterior TRNs show decreases in velocity and acceleration, and an increase in probability of pauses and reversals [4,6,10,34,39], and the posterior TRNs show an increase in acceleration [4,10,34]. It should be noted that we do not measure expression levels of ChR2 in the sensory systems, and any differences in computed filters could be explained by differences in expression levels. However, when assuming uniform expression levels across the sensory systems, our results provide spatiotemporal receptive fields for these systems that are consistent with previous findings [6].

The linear filters resulting from our method provide several insights into the circuitry and morphological differences between the two sensory systems. First, although we used identical stimuli for both segments, the filters produced from activating the anterior TRNs were much more robust than the filters from activating the posterior TRNs, suggesting that downstream interneurons in this circuit are more responsive to the anterior neurons. This preference in downstream activity has also been observed in experiments involving tap responses, which show that reversals dominate over accelerations when tapping cultured plates, and this preference occurs downstream of sensory neuron activity [10]. In contrast, the filters for the posterior segments of PVD were more robust than the anterior segments. This is also consistent with previous findings that show PVD is required for posterior harsh touch sensation, but not required for anterior harsh touch [9]. A key difference in our experiments is that we bypass mechanoreceptor activation, and can therefore ignore differences in sensory neuron response to different spatial stimuli, as well as other neurons that might affect response rate. Therefore, the differential decision making observed in our experiments suggest that the two sensory systems have different strengths of connections to postsynaptic command interneurons. Particularly for PVD, although the

number of physical synapses to forward command neuron PVC and backward command neuron AVA are similar [42], the functional connectivity seems to be higher for PVC compared to AVA.

Our results also provide insight on the levels of spatial encoding in the TRNs and PVD systems. The TRNs, which employ a tiled network to cover the body, appear to have more spatial encoding. When comparing the computed filters for the anterior and posterior TRNs, most behaviors show opposite directions of response. Furthermore, when analyzing this system in four segments, each segment produced a unique set of linear filters. In contrast, the branched network in PVD does not appear to spatially encode behavioral responses. The filters from activating the anterior and posterior segments of the PVD system have similar dynamics, with the anterior filters having slightly smaller magnitudes and longer delays. This contrast between the two systems suggests that although both the TRNs and PVDs have spatially distributed processes to sense touch throughout the body, the unique morphological strategies in the two systems lead to differences in their capabilities of encoding responses. Biologically, this disparity in encoding can be explained by their morphologies, as the tiled TRN system consists of more nodes, which could allow for more specific behavioral responses.

Lastly, we investigated the role of the cryptic PVM neuron. Although shown to respond to mechanical stimuli [32], its role in mediating behavior is poorly understood [4,6,10,34]. We found that activating PVM did not induce significant changes in velocity, but induced a slight decrease in acceleration. Interestingly, PVM activation significantly reduced the probability of reversal events. These filters suggest a unique function for PVM in modulating escape response. In contrast to the other TRNs, PVM does not induce escape responses, but rather suppresses these behaviors, as well as decrease the velocity of forward movement.

These findings demonstrate the utility of our method for providing new insights into the dynamics of the mechanosensory system in *C. elegans*, one of the earliest and most morphologically characterized neural circuits. By using a quantitative framework to compare the dynamics between the two sensory systems, we captured properties that are supported by previous literature, and provide further insights in the temporal and spatial encoding in these systems. Additionally, we used linear filters computed from BWA to create LNE models that accurately predict the behavioral responses of animals in response to activity in sensory neurons alone. Because this method is noninvasive and independent of natural stimulus, it can

be easily extended to investigate the dynamics of other neural circuits in *C. elegans* and other model organisms.

Acknowledgments

The authors gratefully acknowledge the funding support of the US National Institutes of Health (R01NS096581, R01GM088333, R21EB021676, and R21EB020424 to HL).

Author Contributions

D.P. and H.L. conceived the project. D.P., J.G., Y.Z. performed experiments and analyzed data. D.P. and H.L. wrote the manuscript with support from all authors.

Methods and Materials

***C. elegans* Maintenance.** We used transgenic worms expressing channelrhodopsin in various mechanosensory neurons. Worm populations were cultured at 20C in the dark on standard nematode growth medium (NGM) petri dishes. Plates were coated with OP50 bacteria lawn supplemented with the cofactor required for channelrhodopsin, all-*trans*-retinal (Sigma-Aldrich). The solution was prepared by diluting a 50mM stock solution (in ethanol) in OP50 suspension to a final concentration of 100uM. Control animals were grown in parallel on OP50 without all-*trans*-retinal. All worms tested were F1 progeny of P0 adults picked onto seeded plates 3-4 days before experiments. Animals were washed to unseeded NGM plates 1hr prior to assays. Animals were then picked to individual plates for experiments. Each animal was exposed to a single stimulus profile and then discarded. The strains used in this work included AQ2334: lite-1(ce314); ljIs123[pmec-4 ChR2; punc-122 RFP] [34] and ZX899: lite-1(ce314); ljIs123[pmec-4 ChR2; punc-122 RFP] [11].

Tracking and Light Delivery Platform. Experiments were performed on a tracking system adapted from a previously developed projector based microscopy system [34]. The system uses an inverted microscope (Leica-DMIRB) with a low-magnification objective (x4) to image freely moving animals. We image using near-infrared light by applying a long-pass filter (715nm) to the transmitted light path and capture images using a large sensor NIR camera (Basler acA2040-180kmNIR), which limits interference in blue light used for optogenetics stimulus. A three-color LCD projector is used as the light source for optogenetic stimulus with selective illumination. We use a camera with large sensor area to capture the full body of the animal, and use a small ROI and binning to reduce the size of images in order to improve processing speed and therefore tracking rate. In order to track individual animals, images taken with the camera are processed to compute the centroid of the animal in terms of x-y pixels on the camera FOV. Based on the position of the computed centroid, a command is sent to a motorized stage to move the animal to the center of the FOV. To apply a light stimulus with spatial and temporal control, we used a modified projector as the light source to the microscope. Images taken with the camera are processed to determine the outline of the animal's body in each frame. The appropriate illumination pattern is then computed and sent to the projector. For each animal, illumination profile and tracking videos were saved for future analysis.

Quantitative Behavior Analysis. To extract quantitative behavioral features from tracking recordings, a custom MATLAB script was used. A series of segmentation and morphological processes were used to extract body postures in each frame. We combined extracted postures with recorded stage movements to quantify several behaviors. We computed various "continuous" behaviors that have a scalar value for each time point. This includes velocity (magnitude), velocity (angle), acceleration, head angle, angular velocity. We also classified various "discrete" behaviors that have been used in previous works [35,36,43,44]. These include behaviors such as pauses, reversals, omega turns, and turns. Each of these behaviors were classified by applying thresholds on quantified continuous behaviors. Pauses and reversals were classified by applying both vertical and horizontal thresholds on velocity measurements. Omega turns were classified by applying a threshold on the eccentricity of the animal's posture. Curves were classified by applying a threshold on the angle of position trajectory.

White Noise Experiments. We used the selective illumination capability of the tracking system to deliver spatially controlled light stimuli to freely moving animals expressing ChR2 in their mechanosensory neurons. We used a pseudorandom m-sequence, a binary signal with unbiased spectrum, similar to a Gaussian white noise signal [15,28]. We tested several white noise signals, and found that an m-sequence with a maximum frequency of 2Hz induced the strongest behavioral responses (data not shown). The generated pseudorandom sequences were repeats of a 6-bit word length m-sequence. We applied the

same pseudorandom signal for each experimental group, applying the signal through the tracking system and changing values in the m-sequence at 2Hz.

Reverse Correlation Analysis. To compute mathematical functions that describe the transformations from sensory neuronal activity into behavior, we first modeled the entire animal as a linear transducer:

$$o(t) = h(t) * s(t) = \int_{-\infty}^{\infty} h(\tau)s(t-\tau)d\tau \qquad (1)$$

Where the relationship between the input signal (neuronal activity through optogenetics) s(t) and output signal (behavior) o(t) is characterized by a function h(t). We used standard reverse-correlation similar to [22,23,26–28], and computed h(t) for specific behaviors by computing a "behavior-weighted-average" (BWA):

$$h(t) \sim BWA = \frac{1}{N}\sum_t \overrightarrow{s_t} \times v_o(t) \qquad (2)$$

Where the stimulus preceding each time-point is weighed by the scalar value of the behavior at that time. For continuous behaviors, we used the scalar values at each time points as the weights. For discrete behaviors, we used a binary signal indicating transitions from forward movement to specific states. For all cases, we compute linear filters using 400 points preceding and following each time point (N = 801).

Nonlinear Filters and Model Predictions. We model static nonlinear filters for each behavioral response in order to extract the nonlinear dynamics not captured in the linear filters computed from reverse correlation [45]. We first compute linear model predictions by convolving the computed linear filters from presented stimuli in each trial used, as shown in equation (1). We then compare these linear predictions to the measured outputs at each time point, and fit a quadratic function. These quadratic functions are then used as the nonlinear filters in a linear-nonlinear (LN) cascade model for specific behavior transformations. We also apply an exponential decay filter (LNE) to capture nonlinear adaptations to the stimuli. Accuracy measurements are computed as R^2 values.

Statistics. Linear filters are presented as mean + SEM as computed by the BWA. The two-tailed Student's t-test was used to compare filter peaks between two groups. $P<0.05$ was considered statistically significant. Accuracy of best-fit nonlinear filters were computed as R^2 values.

Code Availability. All custom code used to generate results in this manuscript are available on Github (https://github.gatech.edu/pages/dporto3/BWA-v1/).

Data Availability. All behavior and stimulus data generated during the current study are available from the corresponding author upon reasonable request.

References:

1. Kandel, E. R., Schwartz, J. H., Jessell, T. M., Siegelbaum, S. A. & Hudspeth, A. J. *Principles of Neural Science, Fifth Edition*. *Neurology* **3,** (2014).

2. White, J. G., Southgate, E., Thomson, J. N. & Brenner, S. THE STRUCTURE OF THE NERVOUS-SYSTEM OF THE NEMATODE CAENORHABDITIS-ELEGANS. *Philos. Trans. R. Soc. London Ser. B-Biological Sci.* **314,** 1–340 (1986).

3. Sengupta, P. & Samuel, A. D. T. Caenorhabditis elegans: a model system for systems

neuroscience. *Curr. Opin. Neurobiol.* **19,** 637–643 (2009).

4. Chalfie, M. *et al.* THE NEURAL CIRCUIT FOR TOUCH SENSITIVITY IN CAENORHABDITIS-ELEGANS. *J. Neurosci.* **5,** 956–964 (1985).

5. Chalfie, M. & Au, M. Genetic control of differentiation of the Caenorhabditis elegans touch receptor neurons. *Science (80-.).* **243,** (1989).

6. Goodman, M. B. Mechanosensation. *WormBook* 1–14 (2006).

7. Albeg, A. *et al.* C-elegans multi-dendritic sensory neurons: Morphology and function. *Mol. Cell. Neurosci.* **46,** 308–317 (2011).

8. Chatzigeorgiou, M. *et al.* Specific roles for DEG/ENaC and TRP channels in touch and thermosensation in C. elegans nociceptors. *Nat. Neurosci.* **13,** 861-U106 (2010).

9. Li, W., Kang, L., Piggott, B. J., Feng, Z. & Xu, X. Z. S. The neural circuits and sensory channels mediating harsh touch sensation in Caenorhabditis elegans. *Nat. Commun.* **2,** (2011).

10. Wicks, S. R., Roehrig, C. J. & Rankin, C. H. A Dynamic Network Simulation of the Nematode Tap Withdrawal Circuit: Predictions Concerning Synaptic Function Using Behavioral Criteria. *J. Neurosci.* **16,** (1996).

11. Husson, S. J. *et al.* Optogenetic Analysis of a Nociceptor Neuron and Network Reveals Ion Channels Acting Downstream of Primary Sensors. *Curr. Biol.* **22,** 743–752 (2012).

12. Abbott, P. D. and L. F. in (The MIT Press, 2001).

13. Simoncelli, E. P., Paninski, L., Pillow, J. & Schwartz, O. *Characterization of Neural Responses with Stochastic Stimuli*. *Cognitive Neurosciences Iii, Third Edition* (2004).

14. Chichilnisky, E. J. A simple white noise analysis of neuronal light responses. *Network-Computation Neural Syst.* **12,** 199–213 (2001).

15. Ringach, D. & Shapley, R. Reverse correlation in neurophysiology. *Cogn. Sci.* **28,** 147–166 (2004).

16. Sharpee, T. O. Computational Identification of Receptive Fields. *Annu. Rev. Neurosci. Vol 36* **36,** 103–120 (2013).

17. Nykamp Siam J Appl Math, D. Q. WHITE NOISE ANALYSIS OF COUPLED LINEAR-NONLINEAR SYSTEMS *. *Soc. Indiustrial Appl. Math.* **63,** 1208–1230 (2003).

18. Hunter, I. W. & Korenberg, M. J. The identification of nonlinear biological systems: Wiener and Hammerstein cascade models. *Biol. Cybern.* **55,** 135–144 (1986).

19. Sakai, H. M. WHITE-NOISE ANALYSIS IN NEUROPHYSIOLOGY. *Physiol. Rev.* **72,** 491–505 (1992).

20. Bredfeldt, C. E. & Ringach, D. L. Dynamics of spatial frequency tuning in macaque V1. *J. Neurosci.* **22,** 1976–1984 (2002).

21. DeAngelis, G. C., Ohzawa, I. & Freeman, R. D. Receptive-field dynamics in the central visual pathways. *Trends Neurosci.* **18,** 451–458 (1995).

22. Ramirez, A. *et al.* Spatiotemporal receptive fields of barrel cortex revealed by reverse correlation of synaptic input. *Nat. Neurosci.* **17,** 866–875 (2014).

23. Behnia, R., Clark, D. A., Carter, A. G., Clandinin, T. R. & Desplan, C. Processing properties of ON and OFF pathways for Drosophila motion detection. *Nature* **512,** 427–430 (2014).

24. Coen, P., Clemens, J. & Weinstein, A. Dynamic sensory cues shape song structure in Drosophila. *Nature* **507,** 233–7 (2014).

25. Clemens, J. *et al.* Connecting Neural Codes with Behavior in the Auditory System of Drosophila. *Neuron* **87,** 1332–1343 (2015).

26. Hernandez-Nunez, L. *et al.* Reverse-correlation analysis of navigation dynamics in Drosophila larva using optogenetics. *Elife* **4,** e06225 (2015).

27. Gepner, R., Mihovilovic Skanata, M., Bernat, N. M., Kaplow, M. & Gershow, M. Computations underlying Drosophila photo-taxis, odor-taxis, and multi-sensory integration. *Elife* **4,** e06229 (2015).

28. Kato, S., Xu, Y., Cho, C. E., Abbott, L. F. & Bargmann, C. I. Temporal Responses of C. elegans Chemosensory Neurons Are Preserved in Behavioral Dynamics. *Neuron* **81,** 616–628 (2014).

29. Suzuki, H. *et al.* In vivo imaging of C-elegans mechanosensory neurons demonstrates a specific role for the MEC-4 channel in the process of gentle touch sensation. *Neuron* **39,** 1005–1017 (2003).

30. Eastwood, A. L. *et al.* Tissue mechanics govern the rapidly adapting and symmetrical response to touch. *Proc. Natl. Acad. Sci. U. S. A.* **112,** E6955-63 (2015).

31. Nekimken, A. L. *et al.* Pneumatic stimulation of C. elegans mechanoreceptor neurons in a microfluidic trap. *Lab Chip* (2017). doi:10.1039/C6LC01165A

32. Cho, Y. *et al.* High-Throughput Controlled Mechanical Stimulation and Functional Imaging In Vivo. *bioRxiv* (2017). doi:https://doi.org/10.1101/107318

33. Shipley, F. B., Clark, C. M., Alkema, M. J. & Leifer, A. M. Simultaneous optogenetic manipulation and calcium imaging in freely moving C-elegans. *Front. Neural Circuits* **8,** (2014).

34. Stirman, J. N. *et al.* Real-time multimodal optical control of neurons and muscles in freely behaving Caenorhabditis elegans. *Nat. Methods* **8,** 153-U78 (2011).

35. Gray, J. M., Hill, J. J. & Bargmann, C. I. A circuit for navigation in Caenorhabditis elegans. *Proc. Natl. Acad. Sci. U. S. A.* **102,** 3184–3191 (2005).

36. Yemini, E., Jucikas, T., Grundy, L. J., Brown, A. E. X. & Schafer, W. R. A database of Caenorhabditis elegans behavioral phenotypes. *Nat. Methods* **10,** 877–+ (2013).

37. Geng, W., Cosman, P., Berry, C. C., Feng, Z. & Schafer, W. R. Automatic tracking, feature extraction and classification of C elegans phenotypes. *IEEE Trans. Biomed. Eng.* **51,** 1811–1820 (2004).

38. Albrecht, D. R. & Bargmann, C. I. High-content behavioral analysis of Caenorhabditis elegans in precise spatiotemporal chemical environments. *Nat. Methods* **8,** 599-U120 (2011).

39. Leifer, A. M., Fang-Yen, C., Gershow, M., Alkema, M. J. & Samuel, A. D. T. Optogenetic manipulation of neural activity in freely moving Caenorhabditis elegans. *Nat. Methods* **8,** 147-U71 (2011).

40. Rose, J. K. & Rankin, C. H. Analyses of habituation in Caenorhabditis elegans. *Learn. Mem.* **8,** 63–69 (2001).

41. Timbers, T. A., Giles, A. C., Ardiel, E. L., Kerr, R. A. & Rankin, C. H. Intensity discrimination deficits cause habituation changes in middle-aged Caenorhabditis elegans. *Neurobiol. Aging* **34,** 621–631 (2013).

42. Altun, Z.F., Herndon, L.A., Wolkow, C.A., Crocker, C., Lints, R. and Hall, D. . WormAtlas. at <http://www.wormatlas.org>

43. Huang, K.-M., Cosman, P. & Schafer, W. R. Automated detection and analysis of foraging behavior in Caenorhabditis elegans. *J. Neurosci. Methods* **171,** 153–164 (2008).

44. Larsch, J., Ventimiglia, D., Bargmann, C. I. & Albrecht, D. R. High-throughput imaging of neuronal activity in Caenorhabditis elegans. *Proc. Natl. Acad. Sci. U. S. A.* **110,** E4266-73 (2013).

45. Korenberg, M. J. & Hunter, I. W. THE IDENTIFICATION OF NONLINEAR BIOLOGICAL-SYSTEMS - LNL CASCADE MODELS. *Biol. Cybern.* **55,** 125–134 (1986).

Figures

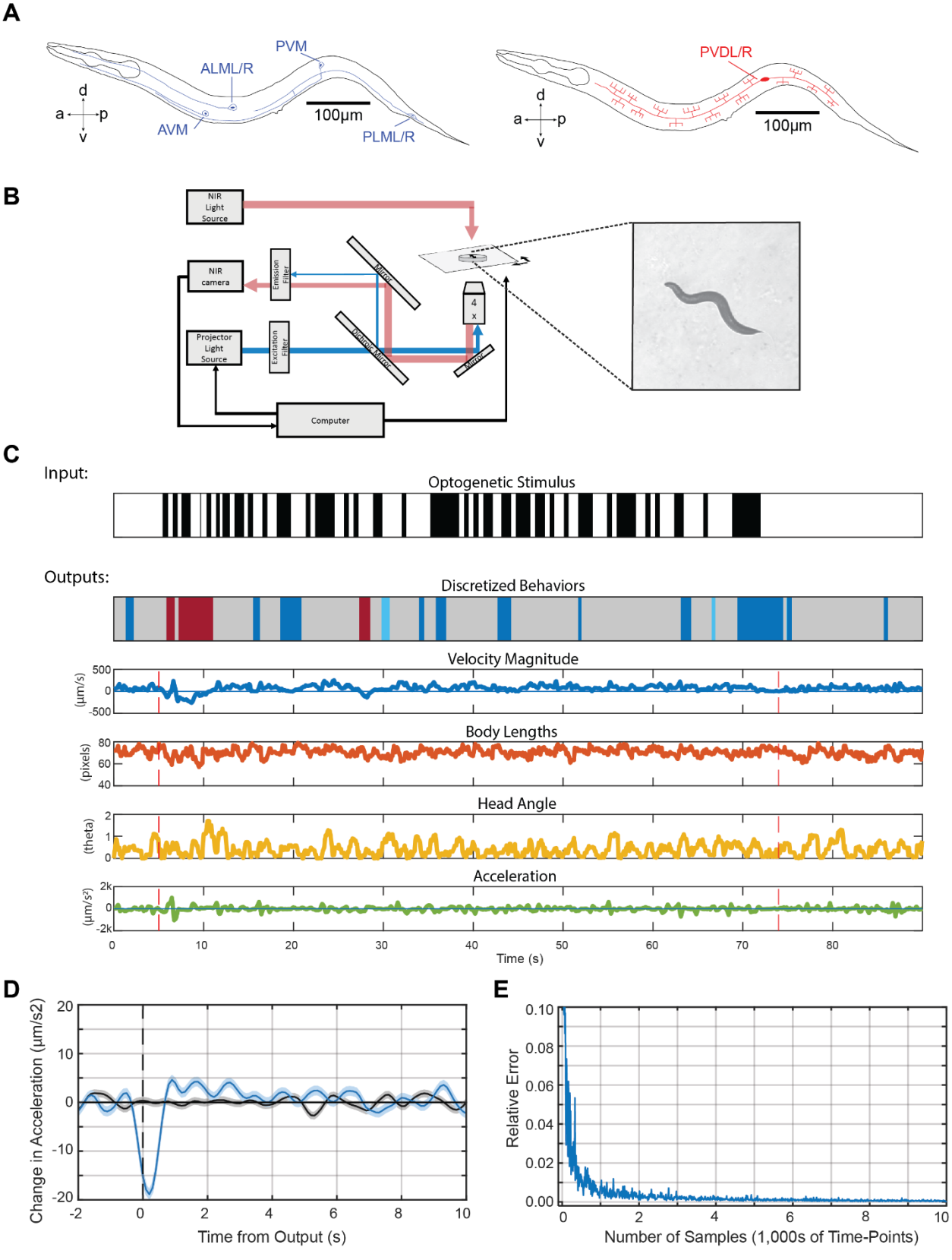
A
PVM
ALML/R
AVM
PLML/R
100µm
d
a
p
v
PVDL/R
100µm
B
NIR Light Source
NIR camera
Emission Filter
Mirror
Projector Light Source
Excitation Filter
Dichroic Mirror
4 x
Mirror
Computer
C
Input:
Optogenetic Stimulus
Outputs:
Discretized Behaviors
Velocity Magnitude
(µm/s)
Body Lengths
(pixels)
Head Angle
(theta)
Acceleration
(µm/s²)
Time (s)
D
Change in Acceleration (µm/s2)
Time from Output (s)
E
Relative Error
Number of Samples (1,000s of Time-Points)

Figure 1: Reverse correlation analysis of mechanosensory neurons enabled by tracking and selective illumination platform.

A) Mechanosensory neurons characterized in this study. The gentle touch sensing neurons ALML/R, AVM, PVM, and PLML/R (blue) and harsh touch sensing neurons PVDL/R (red).
B) Custom tracking system with selective illumination used for reverse correlation experiments (Methods).
C) Sample stimulus and behavior traces obtained from the custom platform and analysis script (Methods).
D) Sample filter computed using BWA computation (n = 88,031).
E) The speed of convergence for the VWA as a function of the amount of data used to train the model. The error converges to a relative tolerance of $\delta<0.005$ after 30,000 time-points.

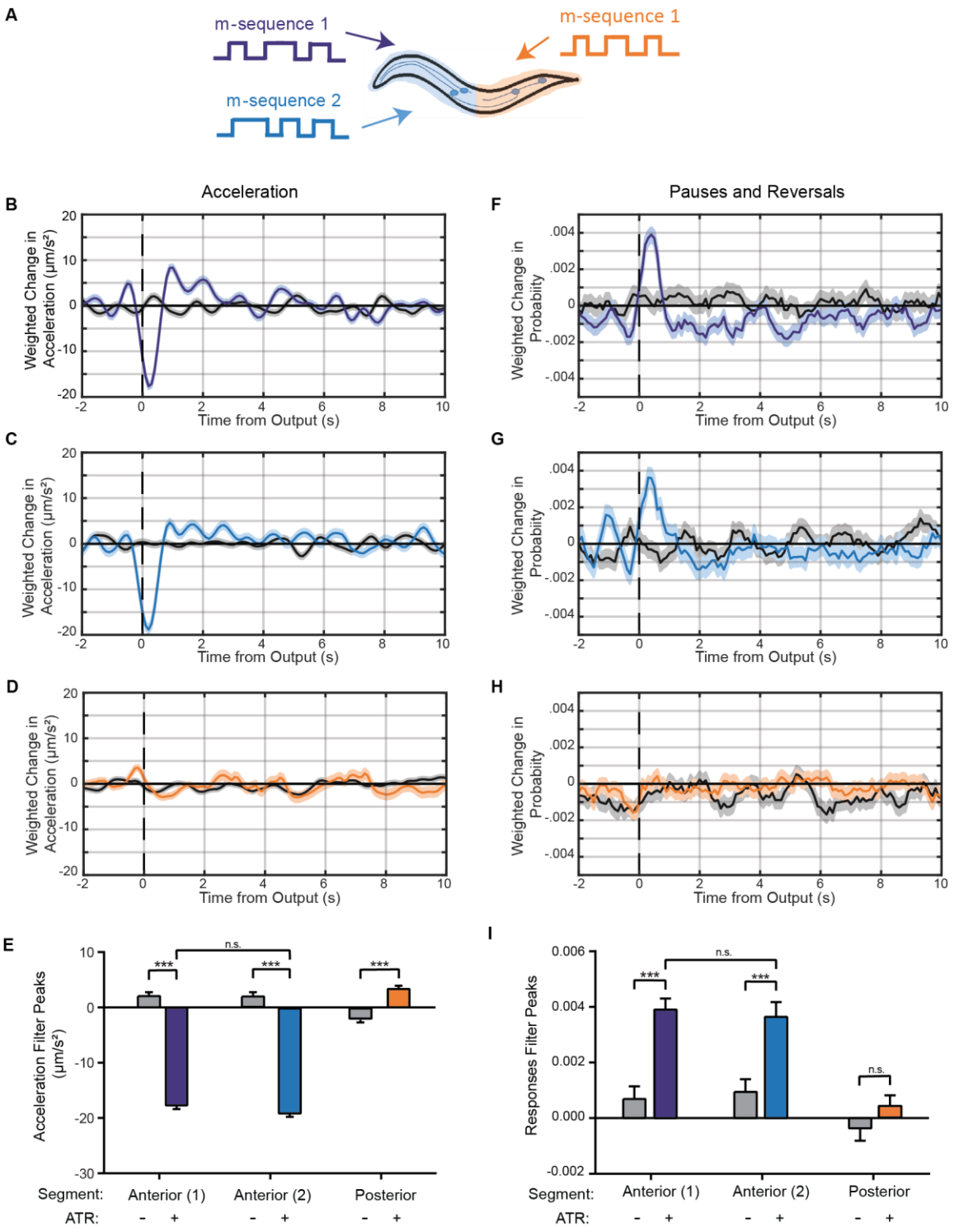

Figure 2: Linear filters for the touch receptor neurons (TRNs) responses are robust and reproducible

A) Schematic of stimulus patterns and TRNs analyzed. Animals express channelrhodopsin using the mec-4 promoter.

B-D) Linear filters computed for acceleration when stimulating the B,C) anterior and the D) posterior TRNs with an m-sequence. Colored plots represent filters computed from ATR-fed animals, black

plots represent filters computed from control (not ATR-fed) animals. Dark line and light shade represent BWA and SEM, respectively (n>36,000 for all conditions, specific values listed in SI Table 1).

E) Comparisons of peak values from computed linear filters in B-D. Error bars indicate SEM. Statistical significance computed using student's t-test (***p<0.001).

F-H) Linear filters computed for pauses and reversals when stimulating the F,G) anterior and the H) posterior TRNs with an m-sequence. Colored plots represent filters computed from ATR-fed animals, black plots represent filters computed from control (not ATR-fed) animals. Dark line and light shade represent BWA and SEM, respectively (n>36,000 for all conditions, specific values listed in SI Table 1).

I) Comparisons of peak values from computed linear filters in F-H. Error bars indicate SEM (n>36,000 for all conditions, specific values listed in SI Table 1). Statistical significance computed using student's t-test (***p<0.001).

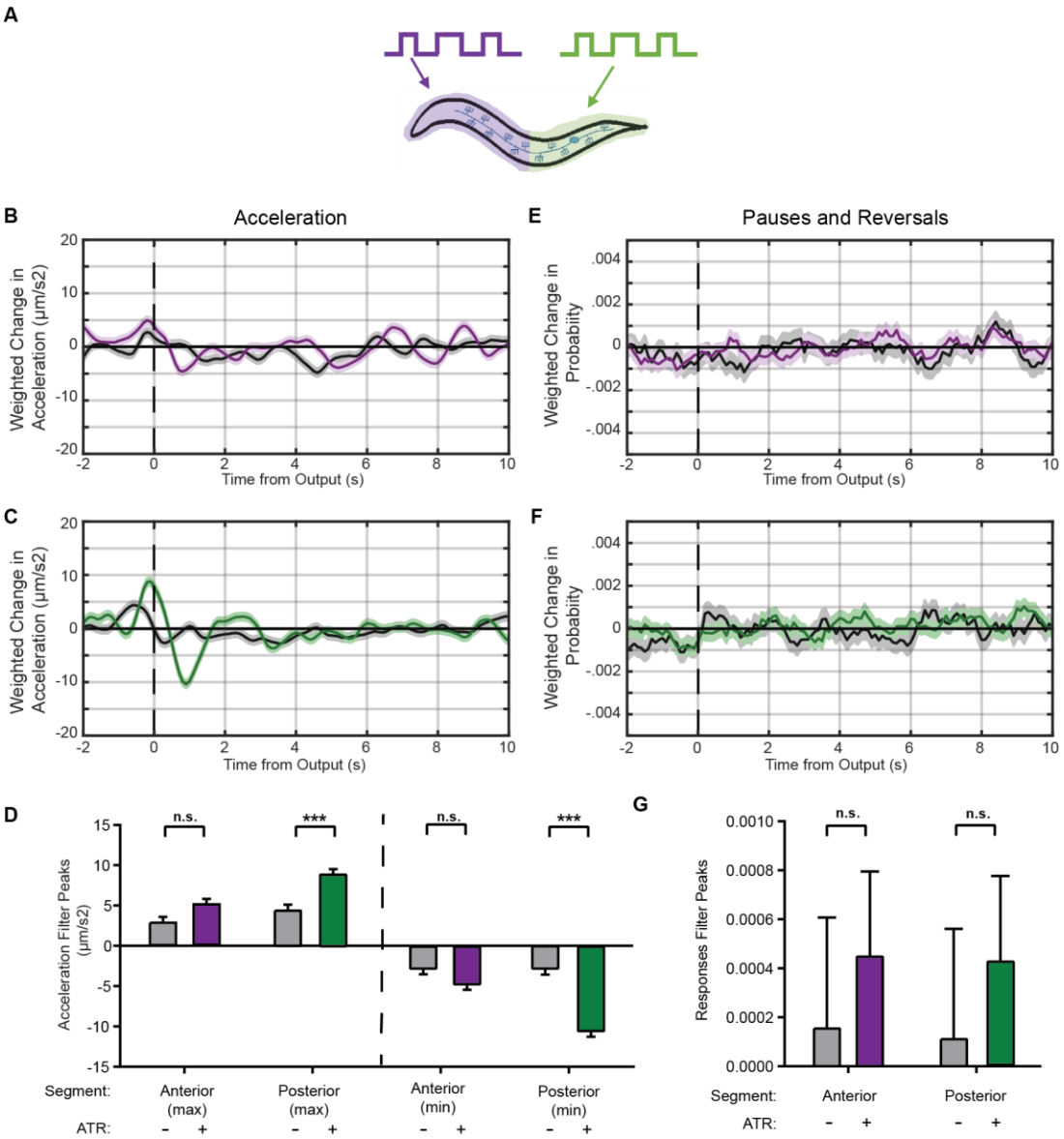

Figure 3: Linear filters for PVD activity illuminate dynamic differences between gentle and harsh touch systems

A) Schematic of stimulation patterns and segments of PVD being characterized.

B-C) Linear filters computed for acceleration when stimulating the B) anterior and C) posterior regions. Colored plots represent filters computed from ATR-fed animals, black plots represent filters computed from control (not ATR-fed) animals. Dark line and light shade represent BWA and SEM, respectively (n>45,000 for all conditions, specific values listed in SI Table 1).

D) Comparisons of peak values from computed filters. Error bars indicate SEM (n>45,000 for all conditions, specific values listed in SI Table 1).

E-F) Linear filters computed for pauses and reversals when stimulating the E) anterior and F) posterior regions. Colored plots represent filters computed from ATR-fed animals, black plots represent filters computed from control (not ATR-fed) animals. Dark line and light shade represent BWA and SEM, respectively (n>45,000 for all conditions, specific values listed in SI Table 1).

G) Comparisons of peak values from computed filters. Error bars indicate SEM (n>45,000 for all conditions, specific values listed in SI Table 1).

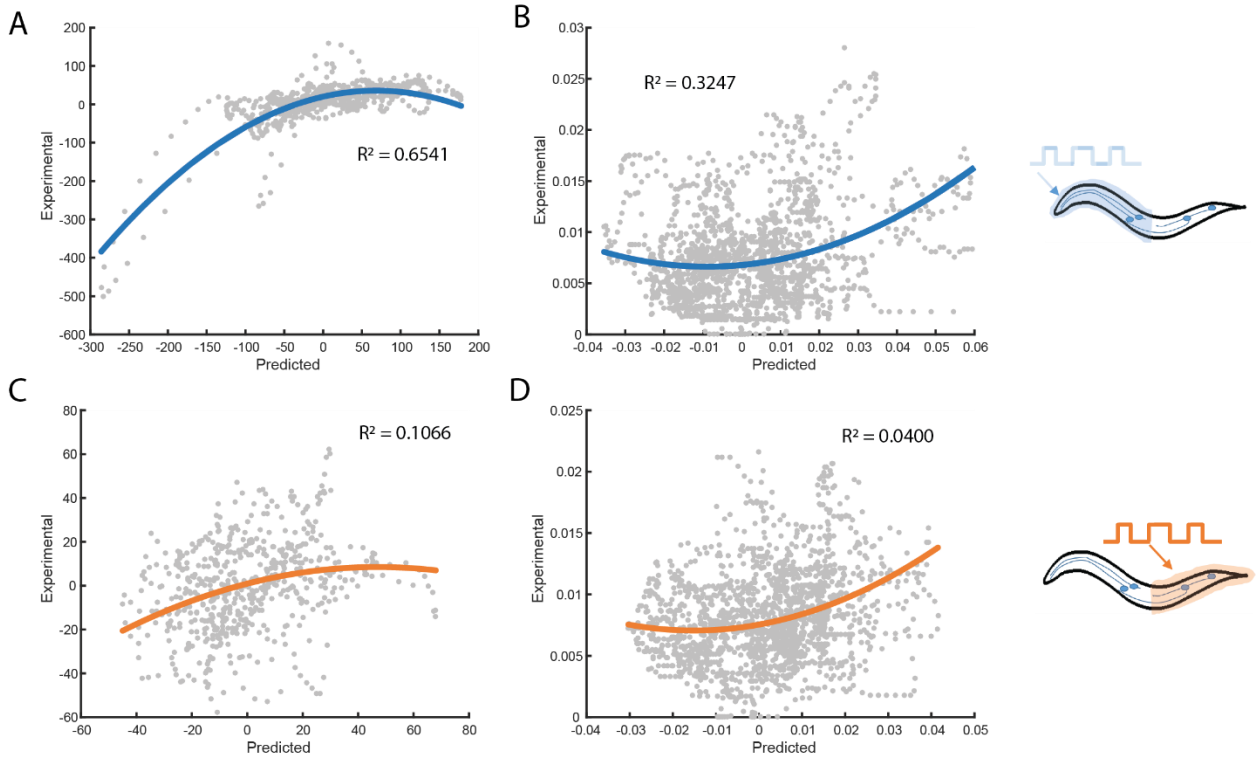

Figure 4: Static nonlinear filters capture nonlinear dynamics in behavioral outputs.
A,B) Nonlinear filters computed for different behaviors when stimulating the anterior TRNs, including A) acceleration and B) transitions into reversals.
C,D) Nonlinear filters computed for different behaviors when stimulating the posterior TRNs, including C) acceleration and D) transitions into reversals. (n>1,730 for all conditions)

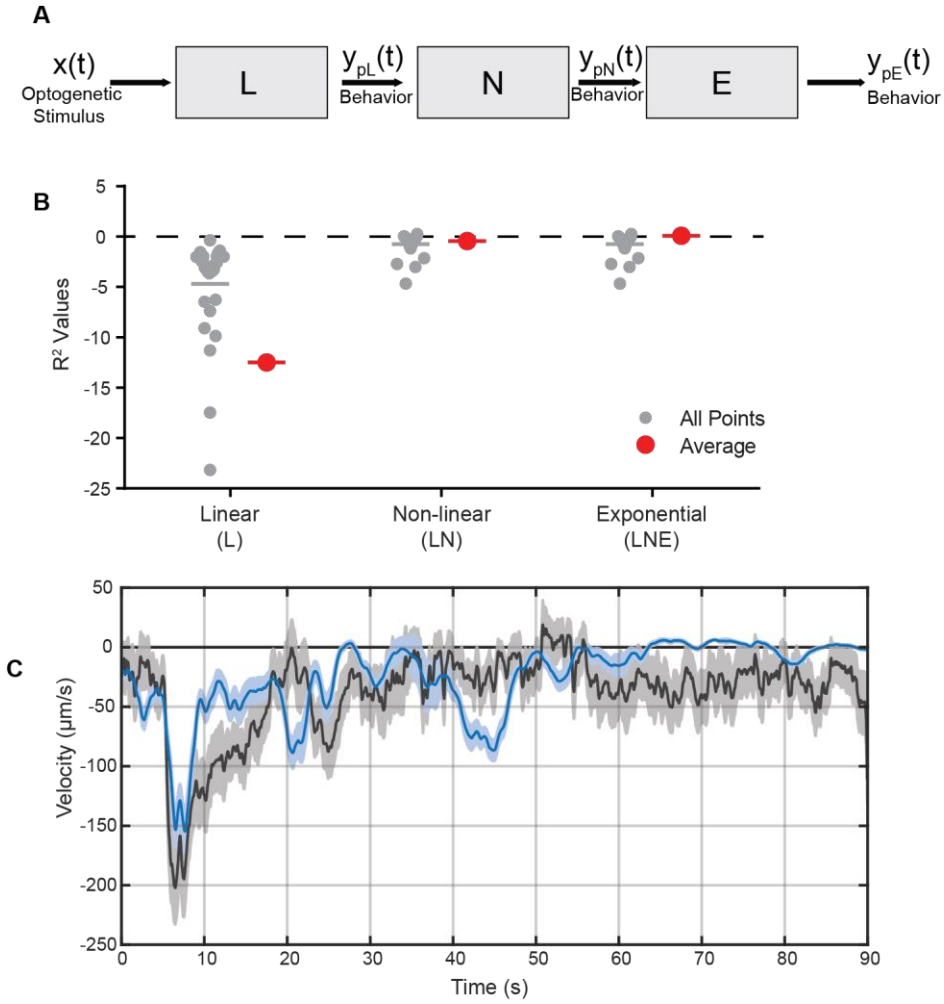

Figure 5: Linear-Nonlinear-Exponential (LNE) model accurately predicts behavioral response

A) Schematic of LNE model for behavioral responses to mechanosensory neuron activity: a LTI system modeled from BWA, followed by a static nonlinear filter and exponential decay filter.

B) Model accuracy values for individual and average traces (n = 31).

C) Comparison of model velocity predictions (blue) and experimental traces (black). Dark line and shade represent average and SEM, respectively (n = 31).

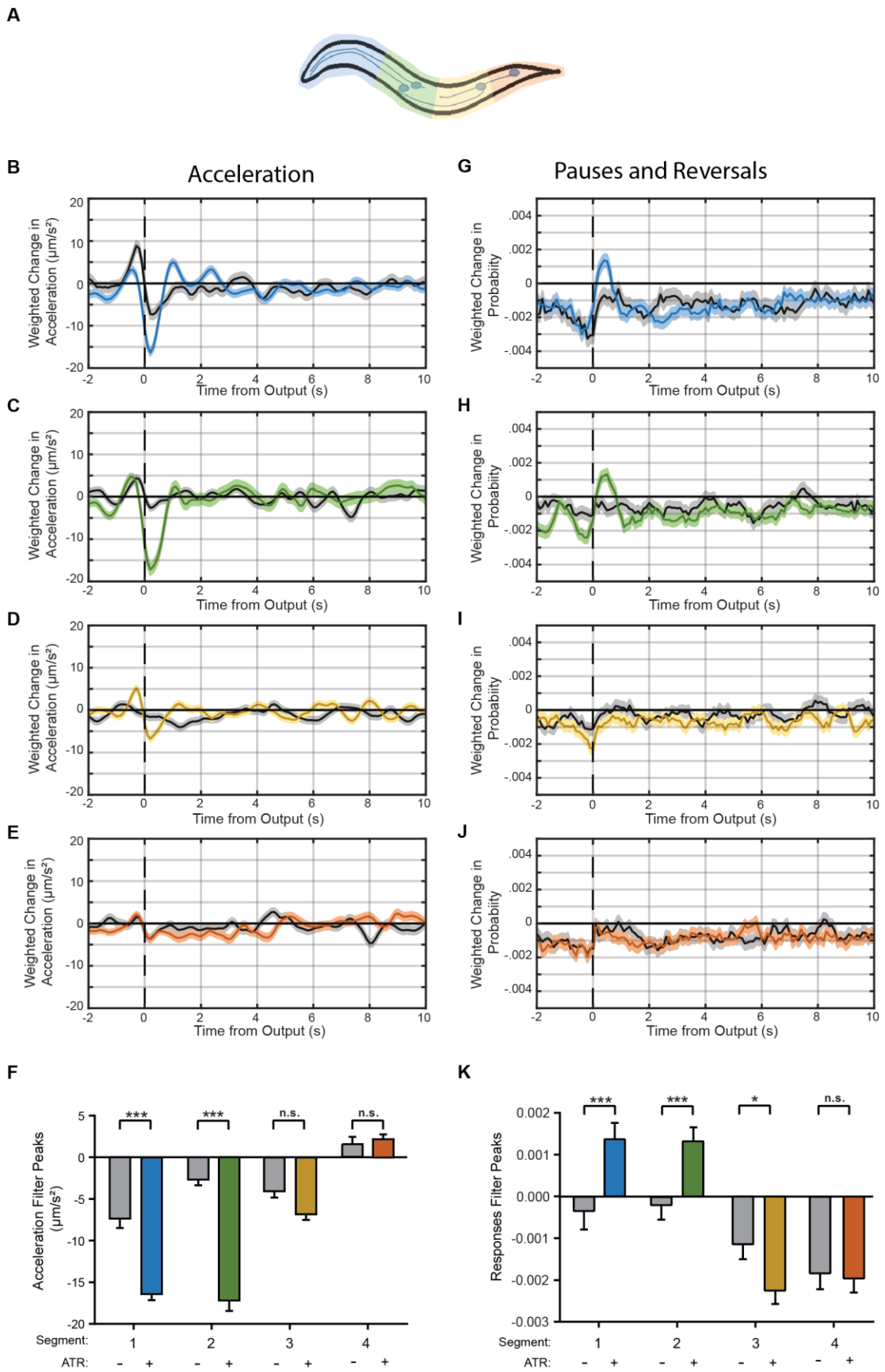
A
B
Acceleration
G
Pauses and Reversals
C
H
D
I
E
J
Weighted Change in Acceleration (µm/s²)
Weighted Change in Probability
Time from Output (s)
F
K
Acceleration Filter Peaks (µm/s²)
Responses Filter Peaks
***
n.s.
*
Segment:
ATR:

Figure 6: Decreasing stimulus region allows for the estimation of a spatiotemporal receptive field with higher resolution

A) Schematic of stimulus patterns and TRNs analyzed.

B-E) Linear filters computed for acceleration when stimulating B) the most anterior, C) the second-most anterior quarter, D) second-most posterior quarter, and E) the most posterior quarter of the TRNs with an m-sequence. Colored plots represent filters computed from ATR-fed animals, black plots represent filters computed from control (not ATR-fed) animals. Dark line and light shade represent BWA and SEM, respectively (n>28,000 for all conditions, specific values listed in SI Table 1).

F) Comparisons of peak values from computed filters in B-E. Error bars indicate SEM (n>28,000 for all conditions, specific values listed in SI Table 1).

G-J) Linear filters computed for acceleration when stimulating G) the most anterior, H) the second-most anterior quarter, I) second-most posterior quarter, and J) the most posterior quarter of the TRNs with an m-sequence. Colored plots represent filters computed from ATR-fed animals, black plots represent filters computed from control (not ATR-fed) animals. Dark line and light shade represent BWA and SEM, respectively (n>28,000 for all conditions, specific values listed in SI Table 1).

K) Comparisons of peak values from computed filters in B-E. Error bars indicate SEM (n>28,000 for all conditions, specific values listed in SI Table 1).